Int J Adv Manuf Technol (2018) 94:1677–1688
DOI 10.1007/s00170-016-9785-8

ORIGINAL ARTICLE

Improved forecasting compensatory control to guarantee the remaining wall thickness for pocket milling of a large thin-walled part

Xinzhi Wang[1] · **Qingzhen Bi**[1] · **Limin Zhu**[1] · **Han Ding**[1]

Received: 17 August 2016 / Accepted: 16 November 2016 / Published online: 28 November 2016

Abstract Pocket milling is widely used in the machining of large thin-walled parts. The remaining wall thickness of the pocket is critical to compromise the weight reduction and the strength, and becomes a crucial dimension requirement during machining. However, the cutting deformation of large thin-walled parts will greatly decrease the accuracy of the remaining wall thickness and needs to be compensated online due to the stochastic characteristics of the deformation. For online compensation methods, the time-delay is usually the critical factor to reduce the control accuracy. The forecasting compensatory control (FCC) provides an effective way to compensate the stochastic errors and solve the time-delay problem. The key of the FCC is the prediction accuracy of the modeling technique. An improved FCC system with an accurate cutting deformation prediction model is developed to guarantee the remaining wall thickness for the pocket milling of a large thin-walled part. The improved FCC system makes use of the advanced online measurement system, the deformation prediction modeling, and the real-time compensation. The proposed prediction model considers the deterministic and stochastic cutting deformations to improve the prediction accuracy. The Kalman filtering is also applied to further enhance the prediction accuracy because of its correctable ability. The cutting simulation and the experiment of machining a rectangular pocket on a large thin-walled plate are both carried out to validate the effectiveness of the proposed method. The accuracy of the remaining wall thickness of the pocket is finally improved.

Keywords Large thin-walled parts · Forecasting compensatory control · Deformation prediction model · Kalman filtering · Remaining wall thickness

✉ Qingzhen Bi
biqz@sjtu.edu.cn

Xinzhi Wang
1130209030@sjtu.edu.cn

Limin Zhu
zhulm@sjtu.edu.cn

Han Ding
hding@sjtu.edu.cn

[1] State Key Laboratory of Mechanical System and Vibration, School of Mechanical Engineering, Shanghai Jiao Tong University, Shanghai 200240, People's Republic of China

Nomenclature

d_k	Real cutting deformation at step k
$\hat{d}_{\bar{k}}$	Forecasted cutting deformation at step k
y_k	Deterministic deformation at step k
z_k	Stochastic deformation at step k
$\hat{z}_{\bar{k}}$	Predicted value of the stochastic deformation at step k
u_k	Control signal at step k
r	Reference signal
$k_{10},k_{20},k_{30},k_{40}$	Stiffness coefficients of two transversal and two rotational elastic springs
k_1,k_2,k_3,k_4	Non-dimensional stiffness coefficients of two transversal and two rotational elastic springs
ρ,A_s,E,I,l,ξ	Parameters related to material and geometry of the beam
x	spatial coordinate along the neutral axis of the beam
$Y_i(\xi)$	ith mode shape of the beam
$q_i(t)$	ith generalized modal coordinate of the beam
W_i	Function representing the ith mode shape of the beam

ω_i	ith natural frequency of the beam
$N_i(t)$	ith generalized force of the beam
$\mathtt{f}$	External force applied on the beam
ω_F	Excitation frequency of the external force
M_i	ith generalized mass of the beam
δ	Deviation between the response of the beam model and the actual cutting deformation
$\delta(\xi - c / l)$	Unit impulse function
$\boldsymbol{s}_k$, $\hat{\mathrm{S}}_k^-$	Real and priori estimate state variable at step k
$\boldsymbol{w}_k$, v_k	Process and measurement noise at step k
p($\boldsymbol{w}$)	State distribution of $\boldsymbol{w}$
N(0, $\boldsymbol{Q}$)	Gaussian distribution with mean 0 and variance $\boldsymbol{Q}$
$\boldsymbol{Q}$, R	Process and measurement noise covariance
$\boldsymbol{K}_k$	Kalman gain at step k
e_k^-	Priori estimate error at step k
$\boldsymbol{P}_k$, $\boldsymbol{P}_k^-$	Real and priori estimate error covariance at step k

1 Introduction

Large thin-walled parts play a key role in the aerospace industry. The geometrical accuracy needs to be strictly controlled in the machining process. Pocket milling is widely used in the machining of large thin-walled parts. The huge fuel tank cylinder is taken as an example. On the inner wall, thousands of pockets should be machined to reduce the weight and improve the transport capacity. The remaining wall thickness of the pocket, which refers to the normal distance between the outer and inner surface of the pocket after machining, is critical to compromise the weight reduction and the strength. The remaining wall thickness becomes a crucial dimension requirement during machining. However, the cutting deformation with stochastic characteristics, which is mainly caused by the weak rigidity of large thin-walled parts, severely decreases the accuracy of the remaining wall thickness.

The cutting deformation is viewed as a deterministic deformation superimposed on a stochastic deformation. Many offline compensation methods are developed to compensate the deterministic cutting deformation. Wan et al. [1] and Ma et al. [2] established the cutting deformation estimation models based on the cutting force modeling methods and compensated the deformation by modifying the tool paths. Some FEA-based models have been developed to predict the force-induced deformations during milling [3–5]. With the help of on-machine measurement (OMM), some error compensation strategies have been proposed to modify the milling paths [6–8]. These methods usually neglect the stochastic deformation which will decrease the accuracy of the large thin-walled part machining.

The online error forecasting and compensation control method is useful to enhance the accuracy of the remaining wall thickness of a large thin-walled part. Li et al. [9–11] proposed a novel flexible fixture that can online monitor and compensate the workpiece deformation during machining. This online adaptive machining gave a typical intelligent method for large workpiece. The method transformed the difficult prediction problem caused by many uncertainty factors such as material inconsistency to the accurate online inspection problem. The machining accuracy can be further improved by solving the time-delay problem of the online technique. The forecasting compensatory control (FCC) [12] is one of the most effective online methods to improve the manufacturing accuracy by compensating the time-delay and considering the stochastic process. Fung et al. [13] implemented the FCC technology based on the linear and non-linear stochastic exogenous autoregressive moving average (ARMAX and NARMAX) models to predict the longitudinal error of a lathe turning and solved the time-delay problem. Precision control in grinder was achieved by integrating the hybrid grey dynamic model into the FCC [14]. Li et al. [15] applied the fuzzy-filtered neural networks into the FCC to estimate the thermal deformation of the spindle and overcame the time lag between the measurement and compensation. The above researches show that the FCC can effectively compensate the time-delay, and the performance of the FCC depends much on the prediction accuracy of the compensation value.

An improved FCC system is developed to guarantee the remaining wall thickness of the rectangular pockets of a large thin-walled part. The prediction model of the improved FCC system considering both the deterministic and stochastic deformations is developed to ensure the accuracy of the modeling technique. Besides, Kalman filtering algorithm [16], which has been proved to be a credible method to improve the prediction accuracy because of its correctable power [17], is also introduced to the improved FCC system. The cutting simulation and experiment finally prove the improved FCC system is effective for the stochastic deformation compensation and solving the time-delay problem. The rest of this paper is organized as follows. The improved forecasting compensatory control system is introduced in Sect. 2. The deformation prediction model is established in Sect. 3. In Sect. 4, the Kalman filtering is employed to improve the prediction accuracy of the stochastic deformation. A simulation and a typical experiment on the pocket milling of a large thin-walled plate are conducted to validate the feasibility in Sect. 5. At last, conclusions of the proposed method are drawn in Sect. 6.

2 Improved forecasting compensatory control system

The main objective of the research is to guarantee the remaining wall thickness of the pockets of a large thin-walled part by

compensating the cutting deformation. The challenge of the deformation compensation is to consider both the deterministic and stochastic deformations. The stochastic deformation is time-variant and difficult to be compensated offline. To compensate the stochastic deformation, the real cutting deformation is monitored using the online measurement system and the compensation is conducted in real-time. Besides, to overcome the time-delay between the measurement and the compensation action, the compensation action is carried out according to the prediction model. Therefore, the prediction accuracy is crucial and directly affects the compensation accuracy. The deformation prediction accuracy is improved based on an accurate deformation prediction model and the Kalman filtering.

The aforementioned compensation control is carried out according to the flowchart in Fig. 1. To solve the time-lag problem, the lag time of the compensation system is chosen as the sampling period, and the deformation of the next period is predicted and used as a compensation value. The compensation control starts with the determination of the real cutting deformation d_{k-1}, which is the difference between the measured and the reference data, and k indicates the kth time instant. The deterministic deformations y_{k-1} and y_k are determined by the deterministic model. Then, the deviation of d_{k-1} and y_{k-1} is used as the stochastic deformation z_{k-1}. Based on the previous and current stochastic deformation, the predicted value of the stochastic deformation $\hat{z}_{\bar{k}}$ is calculated through the stochastic model and the Kalman filtering. The forecasted deformation $\hat{d}_{\bar{k}}$ is determined by $\hat{z}_{\bar{k}}$ and y_k. Finally, according to the forecasted deformation $\hat{d}_{\bar{k}}$, the compensator is controlled to compensate.

The structure of the improved FCC system is shown in Fig. 2. The system is implemented on a mirror milling machine tool, which has two sides of manipulators. One manipulator is used to perform the milling, while the other is used as a support at the opposite side of the machining surface. Three foremost elements are included in this control system: the online measurement system, the deformation predictor, and the compensation system. As mentioned before, the compensation accuracy relies much on the prediction accuracy. Therefore, the deformation predictor is the core part of the control system. To enhance the prediction accuracy of the predictor, two strategies are applied. Firstly, the cutting deformation is viewed as a deterministic deformation superimposed on a stochastic deformation. The deterministic deformation is predicted by a general deformation model for beams, and the stochastic deformation is predicted by an autoregressive integrated moving average (ARIMA) model. Due to the randomness caused by the weak rigidity of the parts and the uncertainties of process parameters, the prediction model considering both the deterministic and stochastic deformations is necessary. Secondly, the Kalman filtering is introduced into the predictor to achieve better prediction precision. According to the Bayes principle, Kalman filtering algorithm can minimize the variation of the estimation error [17]. Therefore, the Kalman filtering can not only predict the cutting deformation but also optimize the established model during machining to approach the actual value.

2.1 Online measurement system

The online measurement system, which is used to obtain the cutting deformation, consists of a laser displacement sensor and a laser controller. The laser displacement sensor is fixed on the supporting head. As such, it has the same linear movement along the X axis as the machining head. The value of D, which represents the distance from the sensor to the workpiece in the Y-direction, can be obtained in real time by using the laser displacement sensor, as shown in Fig. 3. As the workpiece and the measurement device are fixed in the X-direction and Y-direction, respectively, the variation of the value D equals the normal deformation of the workpiece during processing. The laser controller collects the signal of the laser displacement sensor and then performs filtering. Finally, the value of D is transmitted from the laser controller to the compensation system.

2.2 Deformation predictor

The deformation predictor is applied to calculate the forecasted deformation considered as the compensation value. The forecasted deformation includes two parts and can be expressed as follows.

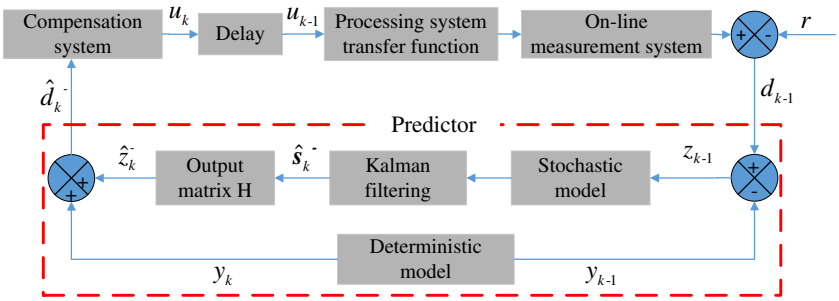

Fig. 1 Design flow of the improved forecasting compensatory control algorithm

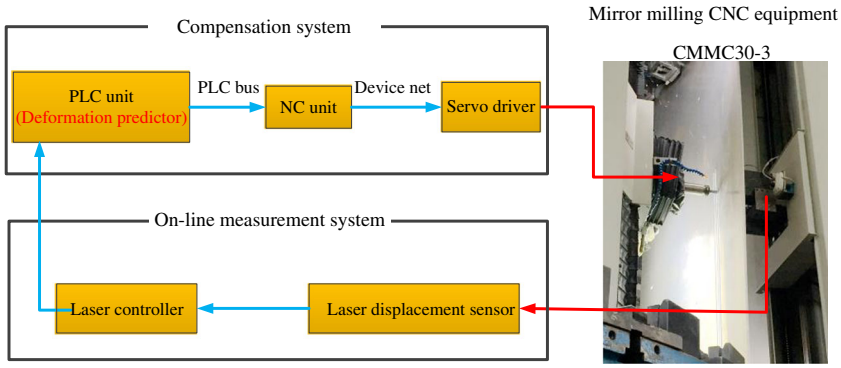

Fig. 2 Structure of the improved forecasting compensatory control system

$$\hat{d}_{\bar{k}} = y_k + \hat{z}_{\bar{k}} \quad (1)$$

The deterministic deformation y_k is calculated by a general deformation model for beams, which will be described in Sect. 3.1. The predicted value of the stochastic deformation $\hat{z}_{\bar{k}}$ is obtained by using the ARIMA model through the Kalman filtering. The establishment of the ARIMA model and the Kalman filtering cycle will be presented in Sects. 3.2 and 4, respectively.

2.3 Compensation system

The compensation system is developed based on the CNC machining system and includes three components: the programmable logic controller (PLC), the numerical controller (NC), and the servo driver. The deformation predictor is integrated in the PLC controlled to give commands for data acquisition and outputting the control signal at a constant interval. During the interval, the cutting deformation and the compensation control signal are collected and calculated, respectively. Then, the compensation control signal is output from the PLC to the NC through the PLC bus. Finally, according to the received signal, the NC offsets the machine coordinate to compensate the cutting deformation and guarantee the remaining wall thickness.

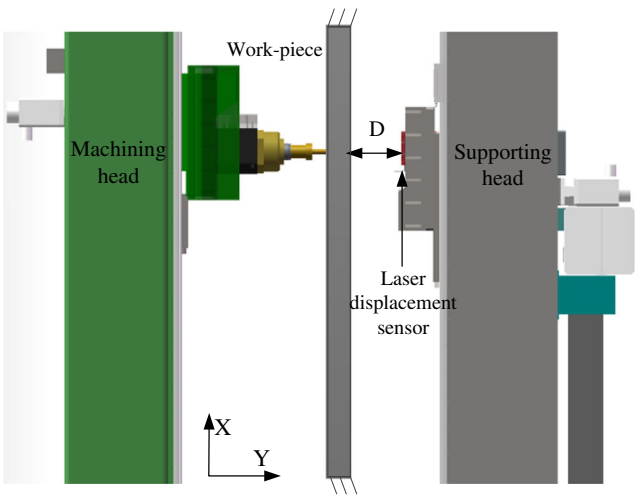

Fig. 3 Schematic of real-time deformation tracking based on the laser displacement sensor

3 Deformation prediction model

Due to the stochastic characteristics of the large thin-walled parts in the milling process, it is of great importance to consider both the deterministic and stochastic cutting deformations. The deterministic and stochastic deformations are viewed as the force-induced error and the deviation between the actual deformation and the response of the deterministic model, respectively. A general deformation model for beams and an ARIMA model are both developed to predict the deterministic and stochastic deformations respectively.

3.1 Deterministic deformation modeling

In the aerospace industry, rectangular pockets can be usually found in some typical large flexible workpieces such as fuel tanks of launch vehicles and aircraft panels. Therefore, the rectangular pocket machining is taken into consideration as a representative of the machining problems in the large thin-walled part milling. Generally, the machining process consists of rough machining and finished machining. In the rough machining of a large thin-walled part, the tool is flexible compared with the workpiece. However, in the finished machining, the workpiece is regarded to be much more flexible than the tool. To predict the force-induced deformation during the finished machining of the pocket of a large thin-walled part, the workpiece model needs to be developed.

The deterministic deformation model for each of the direction-parallel tool paths, which are generated to machine the rectangular pocket, is developed separately. To achieve the above objective, the boundary conditions representing the effect of clamps at both ends and the constraint force of the plane around the milling region can be substituted by two transversal and two rotational elastic springs. Therefore, the deterministic deformation of the direction-parallel tool path can be represented by the transversal deformation of a beam restrained with two transversal and two rotational elastic springs, as depicted in Fig. 4.

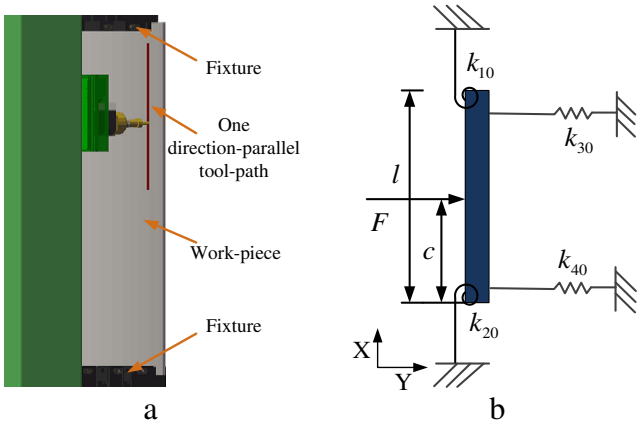

Fig. 4 One cutting process of the direction-parallel tool paths. **a** Machining condition and **b** simplified model

3.1.1 Workpiece mathematical model

A general model for transversal deformation of the beam restrained with two transversal and two rotational elastic springs [18] is used to represent the deterministic deformation of the workpiece. Based on the Euler-Bernoulli assumptions, the transversal deformation of a beam is described by the following equation:

$$\rho A_s \frac{\partial^2 y}{\partial t^2} + EI \frac{\partial^4 y}{\partial x^4} = \mathrm{f} \tag{2}$$

where ρ is the beam density, $A_s$is the beam cross-sectional area, E is the Young's modulus of elasticity, I is the cross-sectional moment of inertia, y represents the transversal deformation, x represents the spatial coordinate along the neutral axis of the beam with length l, and f represents the applied force.

According to the modal superposition principle, the solution of Eq. (2) can be expressed as

$$y(\xi, t) = \sum_{i=1}^{\infty} Y_i(\xi) q_i(t) \tag{3}$$

where $\xi = x/l$, $Y_i(\xi)$ is the ith mode shape of the beam and $q_i(t)$ is the ith generalized modal coordinate. $Y_i(\xi)$ (Eqs. (25) and (26), Appendix) is determined by satisfying the boundary conditions as follows.

For force balance,

$$\left.\frac{\partial^2 Y_i(\xi)}{\partial \xi^2}\right|_{\xi=0} - k_1 \left.\frac{\partial Y_i(\xi)}{\partial \xi}\right|_{\xi=0} = 0, \quad \left.\frac{\partial^2 Y_i(\xi)}{\partial \xi^2}\right|_{\xi=1} + k_2 \left.\frac{\partial Y_i(\xi)}{\partial \xi}\right|_{\xi=1} = 0 \tag{4}$$

For moment balance,

$$\left.\frac{\partial^3 Y_i(\xi)}{\partial \xi^3}\right|_{\xi=0} + k_3 Y_i(\xi)\Big|_{\xi=0} = 0, \quad \left.\frac{\partial^3 Y_i(\xi)}{\partial \xi^3}\right|_{\xi=1} - k_4 Y_i(\xi)\Big|_{\xi=1} = 0 \tag{5}$$

where $k_1 = k_{10}l/(EI)$; $k_2 = k_{20}l/(EI)$; $k_3 = k_{30}l^3/(EI)$; $k_4 = k_{40}l^3/(EI)$; and k_{10}, k_{20}, k_{30}, and k_{40} are the stiffness coefficients of the springs as shown in Fig. 4. As mentioned above, $Y_i(\xi)$ can be represented by a function of the stiffness coefficients of the springs.

$$Y_i(\xi) = \mathrm{W}_i(k_{10}, k_{20}, k_{30}, k_{40}, \xi) \tag{6}$$

where W_i is the function representing the ith mode shape of the beam $Y_i(\xi)$.

According to the Lagrange equation, $q_i(t)$ is obtained by solving the following decoupled system equation [19].

$$\ddot{q}_i(t) + \omega_i{}^2 q_i(t) = N_i(t) \tag{7}$$

where ω_i is the ith natural frequency of the beam.

The machining process model is shown in Fig. 4. The mode shape $Y_i(\xi)$ can be determined as mentioned above. The machining force and the supporting force exerted at the opposite side of the machining surface are assumed to be represented by an external force. The external force is given as

$$f(\boldsymbol{\xi}, t) = \delta(\boldsymbol{\xi} - c/l) F = \boldsymbol{\delta}(\boldsymbol{\xi} - c/l) F_0 \boldsymbol{sin}(\omega_F t) \tag{8}$$

where ω_F is the excitation frequency of the external force. The ith generalized force can be obtained as follows:

$$N_i(t) = \frac{1}{M_i} \int_0^1 Y_i(\xi)\, \mathrm{f}(\xi, t) d\xi = \frac{1}{M_i} Y_i(c/l) F_0 sin(\omega_F t) \tag{9}$$

where M_i is the ith generalized mass. Based on Eqs. (7) and (9), the value of $q_i(t)$ with zero initial conditions can be formulated as below:

$$\begin{aligned} q_i(t) &= \frac{1}{\omega_i} \frac{F_0}{M_i} Y_i(c/l) \int_0^t sin(\omega_F \tau) sin\omega_i(t - \boldsymbol{\tau}) d\tau \\ &= \frac{F_0 Y_i(c/l)}{M_i(\omega_i{}^2 - \omega_F{}^2)} \left(sin(\omega_F t) - \frac{\omega_F}{\omega_i} sin(\omega_i t) \right) \end{aligned} \tag{10}$$

By inserting Eq. (10) into Eq. (3), the dynamic response of the beam at the force-bearing point is computed as

$$y(c/l, t) = F_0 \sum_{i=1}^{\infty} \frac{1}{M_i(\omega_i{}^2 - \omega_F{}^2)} Y_i{}^2(c/l) \left(sin(\omega_F t) - \frac{\omega_F}{\omega_i} sin(\omega_i t) \right) \tag{11}$$

Owing to the low frequency of the servo compensation and the small amount of memory in the numerical control system, static deflection instead of dynamic vibration is considered. Therefore, the external force is static and the excitation frequency $\omega_F << \omega_i$. Based on Eqs. (6) and (11), the static deformation of the beam at the force-bearing point can be obtained as

$$y(c/l, t) = F_0 \sum_{i=1}^{\infty} \frac{1}{M_i \omega_i{}^2} W_i{}^2(k_{10}, k_{20}, k_{30}, k_{40}, c/l) \tag{12}$$

3.1.2 Workpiece model identification

To ensure the accuracy of the beam model, the stiffness coefficients of the springs k_{10}, k_{20}, k_{30}, and k_{40} need to be identified offline. The offline identification for the stiffness coefficients is conducted by minimizing the deviation δ between the response of the beam model and the actual cutting deformation at the calibration points. To avoid solution trapping at local optima, the genetic algorithm [20] is used to acquire the optimum stiffness values of the springs. The objective function to be minimized is presented as follows:

$$\delta = \boldsymbol{min} \sum_{j=1}^{m} \left(d_j - y_j\right)^2 \tag{13}$$

where m is the number of points for the calibration. The identification procedures can be repeated for all the direction-parallel tool paths of the pocket, if needed.

3.2 Stochastic deformation modeling

To model the stochastic process, many mathematical modeling methods, like autoregressive integrated moving average (ARIMA) model [13, 21] and grey model [14, 22], have been used. ARIMA [23] has been widely used because of its prediction power in stochastic process. ARIMA (5,0,0), extended to five previous observations, is employed to represent the stochastic process of the cutting deformation.

$$z_{k+1} = a_1 z_k + a_2 z_{k-1} + a_3 z_{k-2} + a_4 z_{k-3} + a_5 z_{k-4} \tag{14}$$

where $a_1, a_2, \ldots a_5$ are the coefficients which are independent of the time variable k.

4 Prediction accuracy improvement with Kalman filtering

The stochastic cutting deformation varies with time and is difficult to be predicted. To guarantee the prediction accuracy of the stochastic deformation, the Kalman filtering is employed. Kalman filtering algorithm, a generalization of the least-square method, is a set of mathematical equations that provides an efficient computational means to estimate the state of a process and minimizes the mean squared error [16].

To estimate the stochastic deformation through the Kalman filtering, it is necessary to develop a state-space expression. According to Eq. (14), we can obtain

$$\begin{bmatrix} z_{k-3} \\ z_{k-2} \\ z_{k-1} \\ z_k \\ z_{k+1} \end{bmatrix} = \begin{bmatrix} 0 & 1 & 0 & 0 & 0 \\ 0 & 0 & 1 & 0 & 0 \\ 0 & 0 & 0 & 1 & 0 \\ 0 & 0 & 0 & 0 & 1 \\ a_5 & a_4 & a_3 & a_2 & a_1 \end{bmatrix} \begin{bmatrix} z_{k-4} \\ z_{k-3} \\ z_{k-2} \\ z_{k-1} \\ z_k \end{bmatrix} \tag{15}$$

Based on Eq. (15), the state-space expression of the stochastic deformation model is given as

$$\begin{cases} \boldsymbol{s}_{k+1} = \boldsymbol{A}\boldsymbol{s}_k + \boldsymbol{w}_k \\ z_k = \boldsymbol{H}\boldsymbol{s}_k + v_k \end{cases} \tag{16}$$

where $\boldsymbol{s}_{k+1} = \begin{bmatrix} z_{k-3} \\ z_{k-2} \\ z_{k-1} \\ z_k \\ z_{k+1} \end{bmatrix}$, $A = \begin{bmatrix} 0 & 1 & 0 & 0 & 0 \\ 0 & 0 & 1 & 0 & 0 \\ 0 & 0 & 0 & 1 & 0 \\ 0 & 0 & 0 & 0 & 1 \\ a_5 & a_4 & a_3 & a_2 & a_1 \end{bmatrix}$,

$\boldsymbol{H} = [0\ 0\ 0\ 0\ 1]$, $\boldsymbol{w}_k$, and v_k represent the process and measurement noise, respectively. $\boldsymbol{w}_k$ and v_k are assumed to be independent of each other and obey a Gaussian distribution, as presented in Eq. (17):

$$\begin{aligned} \mathrm{p}(\boldsymbol{w}) &= \mathrm{N}(0, \boldsymbol{Q}) \\ \mathrm{p}(v) &= \mathrm{N}(0, R) \end{aligned} \tag{17}$$

where $\mathrm{p}(\boldsymbol{w})$ is the state distribution of $\boldsymbol{w}$, $\boldsymbol{Q}$ is the process noise covariance, and R is the measurement noise covariance. The tuning of the filter parameters $\boldsymbol{Q}$ and R is performed offline with the help of system identification. In general, the tuning can acquire statistically superior performance [24].

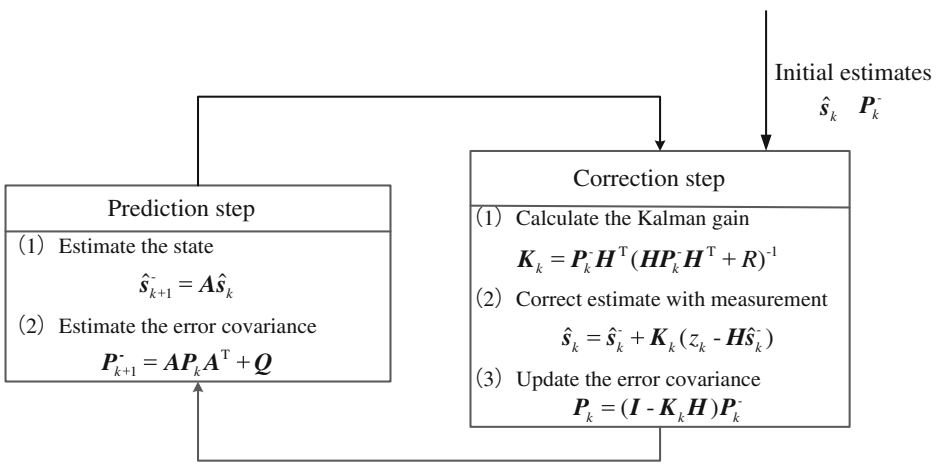

Fig. 5 The Kalman filtering cycle [24]

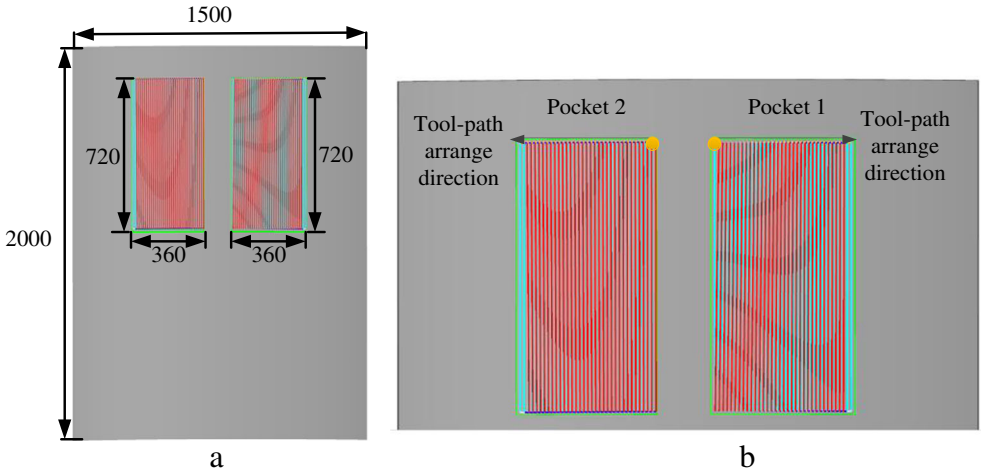

Fig. 6 **a** Integral drawing and **b** partial enlargement drawing of the workpiece for machining (unit: mm)

After obtaining the state-space expression, the Kalman filtering cycle is built as shown in Fig. 5. The cycle is divided into two steps: state prediction and correction. First, the initial estimates $\hat{S}_k^-$ and P_k^- need to be set as follows:

$$\begin{aligned} e_k^- &= s_k - \hat{s}_k^- \\ P_k^- &= \mathrm{E}\left[e_k^- e_k^{-\mathrm{T}}\right] \end{aligned} \tag{18}$$

where $\hat{s}_k^-$ is the priori state estimate at step k given knowledge of the process prior to step k, e_k^- is the priori estimate error, and P_k^- is the priori estimate error covariance. In the correction stage, the Kalman gain $\boldsymbol{K}_k$ is computed by the minimization of the posteriori error covariance $\boldsymbol{P}_k$. Then, the posteriori state estimate $\hat{\boldsymbol{s}}_k$ is corrected with the measured data z_k. Finally, the priori estimate error covariance $\boldsymbol{P}_{k+1}^-$ and the priori state estimate $\hat{\boldsymbol{s}}_{k+1}^-$ are forecasted in the prediction stage. After one correction-prediction cycle, the predicted value of the stochastic deformation $\hat{z}_{k+1}^-$ can be obtained as $\hat{z}_{k+1}^- = H\hat{s}_{k+1}^-$.

5 Verification of the proposed method

The structure of the experimental system is illustrated in Fig. 2. This system consists of a mirror milling CNC equipment CMMC30-3, a compensation system and an online measurement system. The compensation system is developed based on a FAGOR 8070 CNC system, and 20 ms is the compensation period. The online measurement system is made of a laser displacement sensor (OPTEX CD5-W85) and a laser controller (CD5A-N). A thin-walled plate 2000 mm high, 1500 mm wide, and 6 mm thick is used as the workpiece, which is shown in Fig.6a. The material of the workpiece is aluminum alloy 7075.

To demonstrate the validity of the proposed method, the finished machining of a pocket of the large thin-walled plate is taken as an example. Firstly, the profile error of pocket 1 and pocket 2 is determined by on-machine scanning and compensated by modifying the tool paths before processing. Secondly, pocket 1 is machined without the proposed online FCC compensation and the normal deformation of the workpiece is obtained during machining. Thirdly, the deformation prediction model and the Kalman filtering cycle are developed based on the normal deformation of pocket 1. To make sure that the machining conditions of pocket 1 and pocket 2 are close, the tool paths of the two pockets are determined as shown in Fig.6b. Furthermore, pocket 2 is machined using the proposed online FCC compensation. At last, the remaining wall thickness of the two pockets is measured using the ultrasonic measuring system. The machining parameters of the processing are given in Table 1.

As shown in Fig. 6b, the measured normal deformation of the first direction-parallel tool path of pocket 2 during machining is used to verify the prediction accuracy of the proposed method in Sect. 5.1. Then, the results of the whole pocket machining obtained from the experiment are presented in Sect. 5.2

Table 1 The machining parameters of the rectangular pockets milling

Parameters	Description
Pocket dimension	700 mm × 360 mm
Nominal thickness	1.1 mm
Spindle speed	8000 r/min
Feed rates	2500 mm/min
Axial depth of cut	1.5 mm
Helix angle	0°
Cutter diameter	18 mm
Number of flutes	2

Table 2 The non-dimensional stiffness coefficients of the springs for the beam model

k_1	k_2	k_3	k_4
2.04	8.57E + 3	8.70E + 4	4.89

5.1 Effectiveness of the proposed method in deformation prediction

Only first-order modal is considered, and the static deformation of the beam at the tool contact point can be expressed as

$$y(\xi) = \frac{Y^2(\xi) F_0}{M_1 w^2} \tag{19}$$

According to Eq. (19), only $Y^2(\xi)$ is a variable and the others are all constants. Therefore, the deterministic deformation $y(\xi)$ equals the value of $Y^2(\xi)$ after normalization. To avoid obtaining other parameters like the machining force and the Young's modulus of elasticity, the value of $Y^2(\xi)$ and the cutting deformation obtained from experiments are both normalized and compared when conducting the offline identification. After the offline identification, the non-dimensional stiffness coefficients of the springs k_1, k_2, k_3, and k_4 are calibrated and summarized in Table 2. Fig. 7 shows that the tendency of the beam model and the measured data are almost consistent. The cutting deformation of the first sample point is nearly zero, because the position of the first sample point is close to the fixture.

Table 3 The comparative analysis of prediction errors

Models	AME	MSE
The beam model	0.027	2.10E−4
The beam model + ARIMA model	2.69E−3	2.67E−5
The beam model + ARIMA model with the Kalman filtering	2.22E−3	1.29E−5

Two criteria, which are used to measure the deviation between the predictions and the eventual outcomes, are used for evaluating the prediction accuracy. The first criterion is the absolute mean error (AME) and given as

$$\boldsymbol{AME} = \frac{1}{n}\sum_{k=1}^{n} \left|\hat{d}_k^{-} - d_k\right| \tag{20}$$

The second criterion is the mean square error (MSE) and given as

$$\boldsymbol{MSE} = \frac{1}{n}\sum_{k=1}^{n} \left(\hat{d}_k^{-} - d_k\right)^2 \tag{21}$$

The two criteria AME and MSE are calculated and compared in Table 3. Compared with the beam model, the beam

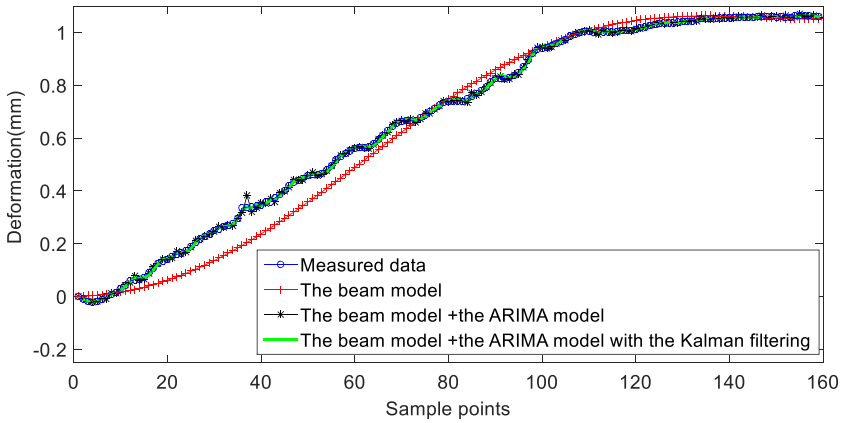

a

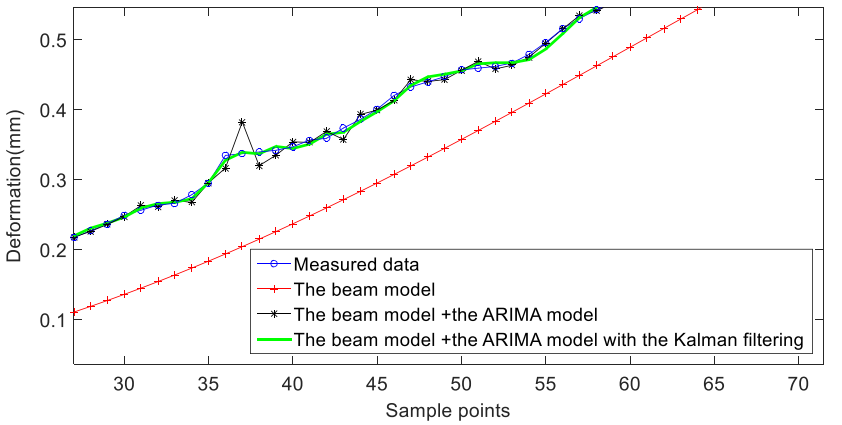

b

Fig. 7 **a** Integral drawing and **b** partial enlargement drawing for estimated profile of the beam model, the beam model + the ARIMA model, and the beam model + the ARIMA model with the Kalman filtering

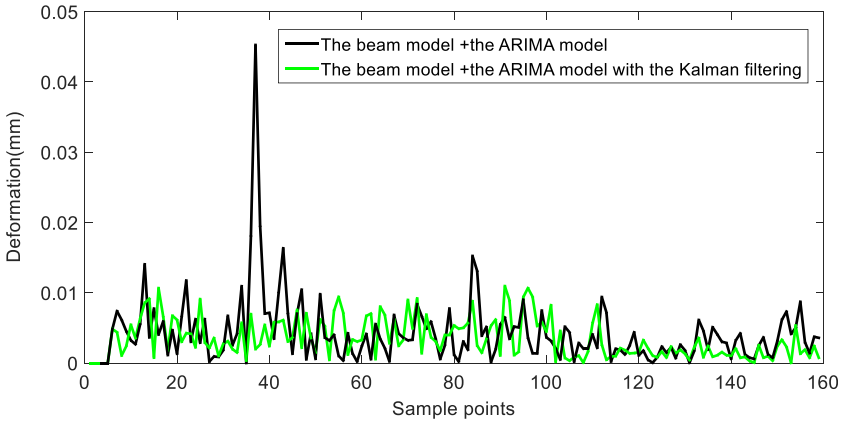

Fig. 8 Absolute residual error of the beam model + the ARIMA model and the beam model + the ARIMA model with the Kalman filtering

model + the ARIMA model can obtain 90.00% and 87.29% reduction in AME and MSE, respectively. Fig. 7 shows the estimated profile of the beam model and the beam model + the ARIMA model. It is seen that the proposed prediction model generates a smaller error than the beam model in the prediction stage, but the prediction accuracy is not satisfactory when original data shows high degree of stochastic uncertainty. Hence, the Kalman filtering is employed to enhance the prediction accuracy. As depicted in Figs. 7 and 8, the proposed prediction model achieves the best prediction accuracy with the help of the Kalman filtering. From the results shown in Table 3, the proposed prediction model with the Kalman filtering can get 17.47% reduction in AME and 51.69% reduction in MSE, in comparison with the proposed prediction model without the Kalman filtering. Furthermore, the proposed method can effectively compensate the time delay as shown in Fig. 9. From the results obtained in this simulation, the proposed method can achieve good prediction accuracy within 0.011 mm.

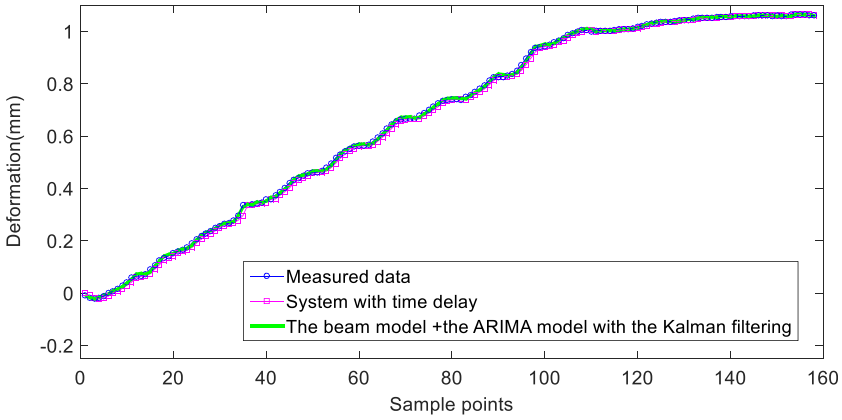

a

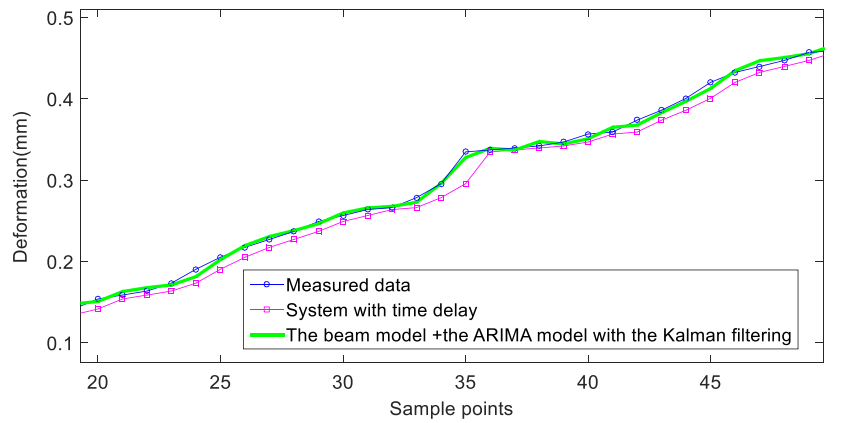

b

Fig. 9 **a** Integral drawing and **b** partial enlargement drawing for estimated profile of the beam model + the ARIMA model with the Kalman filtering and system with time delay

5.2 Effectiveness of the proposed method in deformation compensation

In this section, cutting experiments of the rectangular pocket during the finished machining are presented and compared to validate the effectiveness of the improved FCC system. Fig. 10a presents the wall thickness error distribution of pocket 1 machined by the conventional machining method. The maximum and minimum wall thickness error is 0.9mm and 0.01 mm, respectively. The upper end of pocket 1 is close to the clamped edge, and the lower end of pocket 1 is close to the middle part of the workpiece. The cutting deformation of the upper area of pocket 1 is much smaller than of the lower area. Therefore, the wall thickness error of the lower area of pocket 1 is larger as shown in Fig. 10a. Fig. 10b shows the wall thickness error distribution of pocket 2 machined with the proposed online FCC compensation. After the compensation, the accuracy of the remaining wall thickness is within the range of 0.1 mm. From the above discussion, the conclusion can be reached that the proposed method can guarantee the remaining wall thickness of the rectangular pockets of a large thin-walled part. The machined pockets on the machine are shown in Fig. 11.

Fig. 11 The machined rectangular pockets of a large thin-walled plate. The *left* pocket is pocket 2 and the *right* one is pocket 1

6 Conclusions

An improved FCC system based on an accurate deformation prediction model and the Kalman filtering is proposed and validated for machining the rectangular pockets of a large thin-walled part. The improved FCC system provides an effective way to guarantee the remaining wall thickness. The prediction accuracy of the FCC is improved by establishing a prediction model based on the beam model and the ARIMA model. The proposed prediction model considers both the force-induced and the stochastic deformations of a large thin-walled part. Higher prediction accuracy is achieved by taking the advantage of correctable power of Kalman filtering algorithm. The proposed method can effectively compensate the time-lag problem and achieve good prediction accuracy within 0.011 mm. A large thin-walled plate has been used to validate the effectiveness of the proposed method. The rectangular pocket milling experiment is conducted on the improved FCC system. After the proposed online FCC compensation, the accuracy of the remaining wall thickness is within the range of 0.1 mm.

Acknowledgements The authors gratefully acknowledge the financial support of the National Natural Science Foundation of China (Grant No. U1537209).

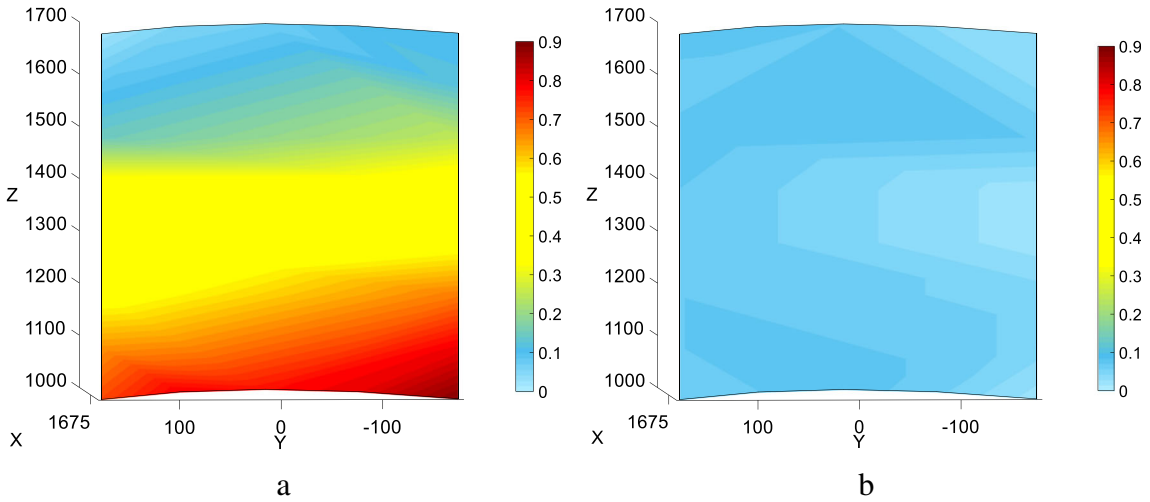

Fig. 10 The wall thickness error distribution of the machined pocket **a** without using the improved forecasting compensatory control and **b** using the improved forecasting compensatory control (unit: mm)

Appendix

The beam mode shapes [18] can be expressed as

$$Y_i(\xi) = C_{1i}sin(r_i\xi) + C_{2i}cos(r_i\xi) + C_{3i}sinh(r_i\xi) + C_{4i}cosh(r_i\xi) \tag{22}$$

where $0 \le \xi \le 1$, $r_i = \sqrt{\alpha_i}$, $\alpha_i = \omega_i \sqrt{\rho A_s l^4/(EI)}$, and C_{1i}, C_{2i}, C_{3i} and C_{4i} are four constants to be determined from the boundary conditions.

By substituting Eq. (22) into the boundary conditions equations, it yields four equations with four constants: C_{1i}, C_{2i}, C_{3i}, and C_{4i}.

$$\begin{aligned}
&k_1 r_i C_{1i} + {r_i}^2 C_{2i} + k_1 r_i C_{3i} - {r_i}^2 C_{4i} = 0\\
&-{r_i}^3 C_{1i} + k_3 C_{2i} + {r_i}^3 C_{3i} + k_3 C_{4i} = 0\\
&\left(r_i k_2 cos(r_i) - {r_i}^2 sin(r_i)\right) C_{1i} - \left(r_i k_2 sin(r_i) + {r_i}^2 cos(r_i)\right) C_{2i}\\
&\qquad + \left(r_i k_2 cosh(r_i) + {r_i}^2 sinh(r_i)\right) C_{3i}\\
&+\left(r_i k_2 \sinh(r_i) + {r_i}^2 cosh(r_i)\right) C_{4i} = 0\\
&\left(k_4 sin(r_i) + {r_i}^3 cos(r_i)\right) C_{1i} + \left(k_4 cos(r_i) - {r_i}^3 sin(r_i)\right) C_{2i}\\
&\qquad + \left(k_4 sinh(r_i) - {r_i}^3 cosh(r_i)\right) C_{3i}\\
&+\left(k_4 cosh(r_i) - {r_i}^3 sinh(r_i)\right) C_{4i} = 0
\end{aligned} \tag{23}$$

The above equation needs to be singular to find the non-trivial solution, and then the natural frequency equation can be obtained as

$$\begin{aligned}
&\left(\alpha_i^2 + k_1 k_3\right)\left(\alpha_i^2 + k_2 k_4\right) - 2\alpha_i\left(\alpha_i^2 k_1 k_2 - k_3 k_4\right) sin\sqrt{\alpha_i} sinh\sqrt{\alpha_i}\\
&+\left[2\alpha_i^2 (k_1 k_4 + k_2 k_3) - \left(\alpha_i^2 - k_1 k_3\right)\left(\alpha_i^2 - k_2 k_4\right)\right] cos\sqrt{\alpha_i} cosh\sqrt{\alpha_i}\\
&-\sqrt{\alpha_i}\left[\left(\alpha_i^3 - k_3 k_4\right)(k_1 + k_2) + \alpha_i(\alpha_i - k_1 k_2)(k_3 + k_4)\right] sin\sqrt{\alpha_i} cosh\sqrt{\alpha_i}\\
&-\sqrt{\alpha_i}\left[\left(\alpha_i^3 + k_3 k_4\right)(k_1 + k_2) - \alpha_i(\alpha_i + k_1 k_2)(k_3 + k_4)\right] cos\sqrt{\alpha_i} sinh\sqrt{\alpha_i} = 0
\end{aligned} \tag{24}$$

After solving for the natural frequencies, the mode shape corresponding to each natural frequency can be determined as follows:

If $B_{0i} \neq 0$

$$\begin{aligned}
Y_i(\xi) = {} & C_{1i} sin(r_i\xi) - C_{1i} B_{1i}/B_{0i} cos(r_i\xi)\\
& + C_{1i} B_{2i}/B_{0i} sinh(r_i\xi) - C_{1i} B_{3i}/B_{0i} cosh(r_i\xi)
\end{aligned} \tag{25}$$

where

$$\begin{aligned}
B_{0i} &= r_i\left(\alpha_i^2 + k_1 k_3\right)\ b_{12} - 2\ k_3 \alpha_i b_{13} + r_i\left(r_i^4 - k_1 k_3\right)\ b_{14}\\
B_{1i} &= r_i\left(\alpha_i^2 + k_1 k_3\right)\ b_{11} + 2\ k_1 \alpha_i^2\ b_{14} + r_i\left(r_i^4 - k_1 k_3\right)\ b_{13}\\
B_{2i} &= r_i\left(\alpha_i^2 + k_1 k_3\right)\ b_{14} + 2\ k_3 \alpha_i b_{11} + r_i\left(r_i^4 - k_1 k_3\right)\ b_{12}\\
B_{3i} &= r_i\left(\alpha_i^2 + k_1 k_3\right)\ b_{13} - 2\ k_1 \alpha_i^2\ b_{12} + r_i\left(r_i^4 - k_1 k_3\right)\ b_{11}\\
b_{11} &= k_2 r_i cos(r_i) - r_i^2\ sin(r_i) \qquad b_{12} = -k_2 r_i sin(r_i) - r_i^2\ cos(r_i)\\
b_{13} &= k_2 r_i cosh(r_i) + r_i^2 sinh(r_i) \qquad b_{14} = k_2 r_i sinh(r_i) + r_i^2 cosh(r_i)
\end{aligned}$$

If $B_{0i} = 0$

$$\begin{aligned}
Y_i(\xi) = {} & -C_{2i}(B_{5i}/B_{4i}) sin(r_i\xi) + C_{2i} cos(r_i\xi) - C_{2i}(B_{6i}/B_{4i}) sinh(r_i\xi)\\
& + C_{2i}(B_{7i}/B_{4i}) cosh(r_i\xi)
\end{aligned} \tag{26}$$

where

$$\begin{aligned}
B_{4i} &= r_i\left(\alpha_i^2 + k_1 k_3\right) b_{41} + 2 k_1 \alpha_i^2 b_{44} + r_i\left(r_i^4 - k_1 k_3\right) b_{43}\\
B_{5i} &= r_i\left(\alpha_i^2 + k_1 k_3\right) b_{42} - 2\ k_3 \alpha_i b_{43} + r_i\left(r_i^4 - k_1 k_3\right) b_{44}\\
B_{6i} &= r_i\left(\alpha_i^2 + k_1 k_3\right) b_{44} + 2\ k_3 \alpha_i b_{41} + r_i\left(r_i^4 - k_1 k_3\right) b_{42}\\
B_{7i} &= r_i\left(\alpha_i^2 + k_1 k_3\right) b_{43} - 2\ k_1 \alpha_i^2\ b_{42} + r_i\left(r_i^4 - k_1 k_3\right) b_{41}\\
b_{41} &= k_4 sin(r_i) + r_i^3 cos(r_i) \quad b_{42} = k_4 cos(r_i) - r_i^3 sin(r_i)\\
b_{43} &= k_4 sinh(r_i) - r_i^3 cosh(r_i) \quad b_{44} = k_4 cosh(r_i) - r_i^3 sinh(r_i)
\end{aligned}$$

References

1. Wan M, Zhang W, Qin G, Wang Z (2008) Strategies for error prediction and error control in peripheral milling of thin-walled workpiece. Int J Mach Tools Manuf 48(12):1366–1374
2. Gao Y-y, Ma J-w, Z-y J, Wang F-j, L-k S, D-n S (2016) Tool path planning and machining deformation compensation in high-speed milling for difficult-to-machine material thin-walled parts with curved surface. Int J Adv Manuf Technol 84(9):1757–1767
3. Rai JK, Xirouchakis P (2008) FEM-based prediction of workpiece transient temperature distribution and deformations during milling. Int J Adv Manuf Technol 42(5):429–449
4. Dong Z, Jiao L, Wang X, Liang Z, Liu Z, Yi J (2016) FEA-based prediction of machined surface errors for dynamic fixture-workpiece system during milling process. Int J Adv Manuf Technol 85(1):299–315
5. Ratchev S, Liu S, Becker A (2005) Error compensation strategy in milling flexible thin-wall parts. J Mater Process Technol 162:673–681
6. Huang N, Bi Q, Wang Y, Sun C (2014) 5-axis adaptive flank milling of flexible thin-walled parts based on the on-machine measurement. Int J Mach Tools Manuf 84:1–8
7. Guiassa R, Mayer JRR, St-Jacques P, Engin S (2015) Calibration of the cutting process and compensation of the compliance error by using on-machine probing. Int J Adv Manuf Technol 78(5):1043–1051
8. Liu HB, Wang YQ, Jia ZY, Guo DM (2015) Integration strategy of on-machine measurement (OMM) and numerical control (NC) machining for the large thin-walled parts with surface correlative constraint. Int J Adv Manuf Technol 80(9):1721–1731
9. Li Y, Liu C, Hao X, Gao JX, Maropoulos PG (2015) Responsive fixture design using dynamic product inspection and monitoring technologies for the precision machining of large-scale aerospace parts. CIRP Ann Manuf Technol 64(1):173–176
10. Li Y, Wang W, Li H, Ding Y (2012) Feedback method from inspection to process plan based on feature mapping for aircraft structural parts. Robot Comput Integr Manuf 28(3):294–302
11. Li Y, Liu C, Gao JX, Shen W (2015) An integrated feature-based dynamic control system for on-line machining, inspection and monitoring. Integr Comput-Aided Eng 22(2):187–200
12. Wu S, Ni J (1989) Precision machining without precise machinery. CIRP Ann-Manuf Technol 38(1):533–536
13. Fung EH, Wong Y, Ho H, Mignolet MP (2003) Modelling and prediction of machining errors using ARMAX and NARMAX structures. Appl Math Model 27(8):611–627
14. Li GD, Yamaguchi D, Nagai M (2007) Application hybrid grey dynamic model to forecasting compensatory control. Eng Comput 24(7):699–711
15. Li Y, Wang M, Hu Y, Wu B (2015) Thermal error prediction of the spindle using improved fuzzy-filtered neural networks. Proc Inst Mech Eng B J Eng Manuf 230:770–778
16. Kalman RE (1960) A new approach to linear filtering and prediction problems. J Basic Eng 82(1):35–45

17. Chui CK, Chen G (2008) Kalman filtering: with real-time applications. Springer Science & Business Media, Berlin
18. Xing J-Z, Wang Y-G (2013) Free vibrations of a beam with elastic end restraints subject to a constant axial load. Arch Appl Mech 83(2):241–252
19. Hanmin S (2006) Vibration system—analyzing, testing, modeling and controlling [M]. Wuhan: Huazhong University of Science and Technology Press, Wuhan
20. Melanie M (1999) An introduction to genetic algorithms. MIT Press, Cambridge
21. Fung EH, Chung AP (1999) Using ARMA models to forecast workpiece roundness error in a turning operation. Appl Math Model 23(7):567–585
22. Li G, Masuda S, Nagai M (2015) Predictor design using an improved grey model in control systems. Int J Comput Integr Manuf 28(3):297–306
23. Box GE, Jenkins GM, Reinsel GC, Ljung GM (2015) Time series analysis: forecasting and control. Wiley, Hoboken
24. Welch G, Bishop G (1995) An introduction to the Kalman filter. University of North Carolina at Chapel Hill, Decatur